Tropical Cyclone Translation Speed and Wind Intensity Effects on Ocean Surface Temperature and Chlorophyll-a

Pia S. Koch , Samuel M. Ayim * , Oliver Wurl

Posted Date: 26 March 2026

doi: 10.20944/preprints202603.2120.v1

Keywords: tropical cyclones; sea surface temperature; chlorophyll-a; translation speed; cold wakes; Indian Ocean

 doi:10.20944/preprints202603.2120.v1

Article

Tropical Cyclone Translation Speed and Wind Intensity Effects on Ocean Surface Temperature and Chlorophyll-a

Pia S. Koch, Samuel M. Ayim * and Oliver Wurl

Center for Marine Sensors (ZfMarS), Institute for Chemistry and Biology of the Marine Environment (ICBM), Carl von Ossietzky Universität Oldenburg, Germany

* Correspondence: samuel.mintah.ayim@uni-oldenburg.de

Highlights

What are the main findings?

- Tropical cyclones with low translation speed (≤ 14.4 km/h) produce the strongest SST cooling (up to - 4 °C) and the largest surface chlorophyll-a anomalies (up to 2 mg m^{-3}).
- The most pronounced SST and chlorophyll-a anomalies occur when slow translation speeds coincide with high wind speeds.

What are the implications of the main findings?

- Under projected climate conditions with slower and more intense tropical cyclones, the Indian Ocean is likely to experience stronger and more persistent SST cooling and phytoplankton responses, with consequences for upper-ocean heat content and air–sea fluxes.
- Effective prediction and impact assessment of cyclone-ocean interactions must account not only for cyclone intensity and translation speed but also for the background ocean state (stratification, barrier layers), to better inform ecosystem management and climate adaptation planning.

Abstract

Tropical cyclones (TCs) are a key component of the Earth system, characterized by extremely intense air-sea interactions. This interaction influences the formation and intensity of TCs and governs biogeochemical processes in the upper ocean. This study investigates whether slower-moving TCs yield stronger Sea Surface Temperature (SST) and chlorophyll-a (Chl-a) anomalies as a response of air-sea interaction. It further examines whether the combination of low translation speed and strong winds induces the strongest cooling and Chl-a anomalies and evaluates the relationship between cold wakes and Chl-a responses. Six TCs of categories 1-5 in the Indian Ocean were analyzed using vertical profiles of temperature from ARGO floats, satellite-derived SST and Chl-a, and meteorological reanalysis data. The results demonstrate that lower translation speed TCs (≤ 14.4 km/h) induced the most significant SST anomalies (-4 °C), and the highest Chl-a anomalies (2 mg m^{-3}). The strongest anomalies occurred when slow translation speeds coincided with high wind speeds. The results indicate that the magnitude of anomalies is sustained not only by translation speed and wind intensity, but also by the stratification of the upper ocean. These contribute to our understanding of the correlation between translation speed, wind strength, atmospheric and oceanic preconditions on SST- and Chl-a anomalies.

Keywords: tropical cyclones; sea surface temperature; chlorophyll-a; translation speed; cold wakes; Indian Ocean

 doi:10.20944/preprints202603.2120.v1

1. Introduction

Tropical cyclones (TCs) are extreme weather events with significant threats to human safety due to their destructive impact on coastlines, infrastructure, and human life [1,2]. TC genesis occurs over the ocean where the Sea Surface Temperature (SST) is higher than 26 °C [3–5]. Beyond their societal impacts, TCs also play a crucial role in regulating processes in the upper layers of the ocean. The vortex motion of TCs can renew the stratification of the ocean through the vertical entrainment and upwelling of cold, nutrient-rich water from the depths [6,7]. This transport of cold, nutrient-rich water can lead to blooms of phytoplankton indicated by chlorophyll-a (Chl-a) anomalies [8]. The magnitude of wind stress is determined by the translation speed, which is defined as the ratio between the local inertial period and the residence time of the TC [7,9]. Thus, translation speed influences the regulation of upwelled nutrients and/or of chlorophyll maxima from the subsurface [9,10]. Previous studies have shown that the coldest SST and highest Chl-a anomalies are measured at low translation speeds (≤ 4 m/s) and high wind speeds [1,8,10]. However, the ocean's response to the passage of a TC is not only dependent on translation speed or wind strength, but also on the ocean's preconditions, subsurface conditions (through eddies, mixed layer, and barrier layer), and the preconditions of the atmosphere [1,8–11]. The Intergovernmental Panel on Climate Change (IPCC) assumes with moderate certainty that TCs will become stronger and intensify more rapidly in the future due to the rise in mean SST, and TCs translation speed will decrease in the future due to weakening atmospheric circulation [1,5,12–15]. Singh and Roxy [1] described the interaction between SST and TC as a two-way process. When SST is high, the ocean enhances the intensity of the TC by transferring heat from the sea to the atmosphere. Upon TC passage, SST cooling generally ranges between 1 °C and 6 °C, occasionally exceeding 10 °C, and can persist for several days to weeks, depending on pre-existing water column stratification [3,7]. As indicated by various studies, not all intense cyclones induce strong phytoplankton blooms [1]. The enhanced Chl-a concentration can result from new production by fueling the surface water with colder, nutrient-enriched deeper water, or in near-shore regions by terrestrial runoff or resuspension of nutrients [3]. Alternatively, the rise of phytoplankton from deeper Chl-a maxima (ibid.). The Chl-a signal can usually be detected three to six days or occasionally up to two to three weeks after TC passage, with Chl-a concentrations between 3 mg m^{-3} to 8 mg m^{-3} [1,3]. This study focuses on the Indian Ocean (IO), which offers favorable conditions for cyclogenesis and the development of TCs [1,16,17]. Several studies have examined the separate effects of TC translation speed and wind intensity on ocean response, but their combined role in modulating SST and Chl-a anomalies in the IO remains unknown. The central objective of this study is to determine whether slower TCs produce stronger SST and Chl-a anomalies and how wind intensity modulates these effects in the IO. The analysis is based on data from ARGO floats and satellite imagery. Accordingly, this study tests the following hypotheses: slower-moving TCs produce stronger SST cooling, the combination of low translation speed and high wind intensity amplifies this cooling, and enhanced SST cooling is associated with a stronger surface Chl-a response.

2. Materials and Methods

The study area is the IO, where one TC developed in the Bay of Bengal, and five TCs in the southern IO (Figure 1). Observations of the selected TCs (Table 1) were obtained from the International Best Track Archive for Climate Stewardship (IBTrACS) [18,19]. These datasets include data on the best track, sustained wind speeds, wind radii, and atmospheric pressure.

For each TC, data were collected from Array for Real-Time Geostrophic Oceanography (ARGO) floats and analyzed for the predefined ROI. ARGO is an international program that uses autonomous profiling floats to monitor the global ocean [3,20]. The ARGO float data were obtained from the Euro-Argo ERIC (European Research Infrastructure Consortium, www.euro-argo.eu/) research platform for fleet monitoring (https://fleetmonitoring.euro-argo.eu/, accessed on July 13, 2025). In this study, the cooling relative to the SST before and after the passage of a TC was determined using ARGO float data. First, a radius was defined for each cyclone, centered on the location of the highest TC intensity,

 doi:10.20944/preprints202603.2120.v1

in which the data from available ARGO floats were obtained and analyzed. Subsequently, these data were categorized by time according to the pre-TC, during-TC, and post-TC schemes. Specifically, pre-TC refers to the 5 days preceding the TC for SST and the 21 days preceding the TC for Chl-a, during-TC corresponds to the duration of the TC itself, and post-TC encompasses the 10–12 days following the TC for SST and the 15–16 days following the TC for Chl-a. The ARGO float data were categorized according to whether they were inside or outside the 34-, 50-, or 64-kt wind radii. For each TC, the temperature data recorded in the upper 100 m of the ARGO float were analyzed. For Anggrek, Marian, and Riley, four indices were necessary due to the longer duration; hence, these TCs included two during-TC periods. To quantify the degree of SST anomalies, the differences between the pre-distinguished time indices were calculated.

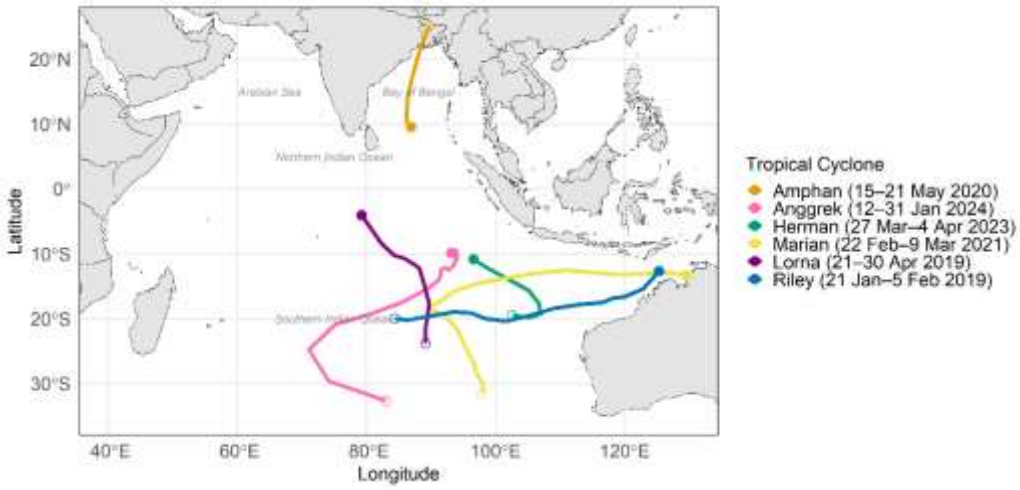

Figure 1. Distribution patterns of analyzed tropical cyclones in the Indian Ocean. Amphan (cat. 5) in the Bay of Bengal (Northern Indian Ocean) in 2020, shown in orange. Anggrek (cat. 4) occurred in the Southern Indian Ocean in 2024 and is illustrated in pink. Herman (cat. 4) evolved in the Southern Indian Ocean in 2023 and is indicated in green. Marian (cat. 3), shown in yellow, developed in the southern Indian Ocean in 2021. Lorna (cat. 2) developed in the Southern Indian Ocean and is illustrated in violet in 2019. Riley (cat. 1) shown in blue occurred in the Southern Indian Ocean in 2019.

Table 1. Analyzed tropical cyclones sorted by Saffir-Simpson (as specified in IBTrACS), including duration, storm ID, region of interest (ROI), and whether they affected the coast.

Name	Category	Timespan	Storm ID	ROI	Coastal Effects
Amphan	5	15.05. – 21.05.2020	2020136N10088	0-25°N, 77-100°E	Yes
Anggrek	4	12.01. – 31.01.2024	42024013S10093	5-35°S, 65-100°E	No
Herman	4	27.03. – 04.04.2023	2023087S10096	9-22°S, 93-110°E	No
Marian	3	22.02. -09.03.2021	2021053S13128	5-10°S, 85-130°E	No
Lorna	2	21.04. – 30.04.2019	2019112S04079	0-27°S, 75-95°E	No
Riley	1	21.01. – 05.02.2019	2019021S09128	5-25°S, 80-130°E	No

The analysis of global daily SST data from 2019 to 2024 was conducted using the product GHRSST (Group for High Resolution Sea Surface Temperature) Level 4 product MUR 0.25° Global Foundation Sea Surface Temperature Analysis (version 4.2) provided by NASA's Jet Propulsion

 doi:10.20944/preprints202603.2120.v1

Laboratory (JPL) via the Physical Oceanography Distributed Active Archive Center (PO.DAAC, https://podaac.jpl.nasa.gov/dataset/MUR25-JPL-L4-GLOB-v04.2, accessed on July 10, 2025) [21]. It facilitates spatially complete global SST fields at a 0.25° spatial resolution [22,23]. Additionally, this product provides an SST anomaly as the difference between the daily SST value and a MUR-based climatology, which is the average for the period from 2003 to 2014 [21]. To depict the cooling caused by TCs in comparison to the usual SST characteristics in the region, the SST anomaly (°C) was used.

To evaluate the possible response of phytoplankton to the passage of observed TCs, satellite-derived surface Chl-a concentrations (mg m^{-3}) were utilized as a proxy for phytoplankton biomass. In contrast, the use of daily data is limited by the restricted availability of cloud-free conditions for remote sensing of surface Chl-a compared to SST [24,25]. Therefore, for the observed period from 2019 to 2024, five-day means of daily satellite images were used from the Ocean-Colour Climate Change Initiative (OC-CCI, version 6.0) provided by the the European Space Agency (www.esa-oceancolour-cci.org, accessed July 10, 2025) [26]. The dataset provides coverage from January 1, 1998 to December 31, 2024, with a spatial resolution of approximately 4 km/pixel (ibid). For each TC, the 25 days preceding its passage were defined as a reference value. The post-TC period was determined based on the duration of the respective bloom. To distinguish the TC-induced Chl-a signal from the typical background variability in the region, a 20-year mean Chl-a climatology was computed for each five-day interval following the TC passages. The difference between the observed values and this long-term average was used to identify possible anomalies due to TC and was expressed as anomalies (in mg m^{-3}).

The MERRA-2 inst6_3d_ana_Np (Modern-Era Retrospective analysis for Research and Applications) was used to identify and analyze large-scale atmospheric structures such as ridges and troughs. The product is provided by the NASA Global Modeling and Assimilation Office (GMAO). It is accessible online through the NASA Goddard Earth Sciences Data Information Services Center (GES DISC, https://disc.gsfc.nasa.gov, accessed July 11, 2025) [27]. The dataset has a resolution of 0.625° × 0.500° and is an instantaneous, three-dimensional, 6-hourly data acquisition [27,28]. This part of the analysis was not performed for all observed TCs, but only for those in which the atmospheric structure appeared to influence TC behavior, for example, in cases of stationary movement or abrupt changes in trajectory. This applied to the TCs Anggrek, Herman, and Marian.

According to Lin [10], a translation speed of $U_h \leq 4$ m/s (14.4 km/h) is considered slow. This threshold value was utilized to analyze the dependence of the observed anomalies (SST and Chl-a) on the translation speed. For the combined group of translation speed and wind speed, the arithmetic mean was used as the threshold value for wind speed (high wind speed ≥ 85.7 km/h).

Therefore, anomalies were computed daily along the trajectory of each TC. As the Chl-a dataset was provided as a five-day mean, linear temporal interpolation was applied to obtain daily values. The extracted anomalies were then combined with the corresponding daily values of the translation speed and exported. Both the SST and Chl-a datasets were subjected to the same set of statistical tests. The Chl-a anomalies along the TC track were linearly interpolated to obtain daily values and merged with the respective TC trajectory. Missing values at the boundaries were replaced with the closest available known values. Statistical analyses were conducted to examine the relationship between the TC-induced anomalies and translation speed. The Shapiro-Wilk test was applied to detect whether the data were normally distributed. A one-way analysis of variance (ANOVA) was performed to examine whether the mean anomalies differed between the groups defined by translation speed and wind intensity. Tukey's HSD tests were then performed to determine which specific group comparisons were statistically significant. The two-sided Wilcoxon Rank-Sum test was used to determine significant differences in anomalies between slow and fast TCs (slow ≤ 14.4 km/h and fast> 14.4 km/h). Statistical tests were based on a significance level of 95%, that is considered to be significant when $p < 0.05$.

All datasets were first subcategorized by region and then processed using the R programming language within the RStudio interface. Grammarly (v1.2.225.1809) was used exclusively as a language

 doi:10.20944/preprints202603.2120.v1

editing tool for correcting spelling and grammar. No prompt-based or generative AI systems were used.

3. Results

3.1. SST Response to Cyclones

Prior to the passage of **Anggrek (Cat 4)**, mixed layer temperature (MLT) in the northeast of the study region was approximately 27.6 °C (ARGO 1902054 (Ascending date: 24.01.2024), Figure 2). The region where Anggrek developed was associated with moderately positive SST anomalies (up to +1.5 °C), while more pronounced cold anomalies (down to -3 °C) appeared southwest of the trajectory (Figure 3a). After the passage of Anggrek, a clear cold wake developed and expanded until January 23 (Figure 3b), with cold anomalies reaching -4 °C (Figure 3b). ARGO 1902054 recorded a cooling of -0.5 °C between January 19 and January 23 (Figure 2). The strongest cooling (-4 °C) occurred in a region in which Anggrek was quasi-stationary and had the lowest translation speed of 2 km/h (Figure 3b). The anomalies observed on January 23 had dissipated by February 10 (Figure 3c). On February 1, ARGO 1902054 recorded a temperature of 28.3 °C, approximately +1.1 °C warmer than the pre-TC conditions, consistent with the observed SST recovery (Figure 3).

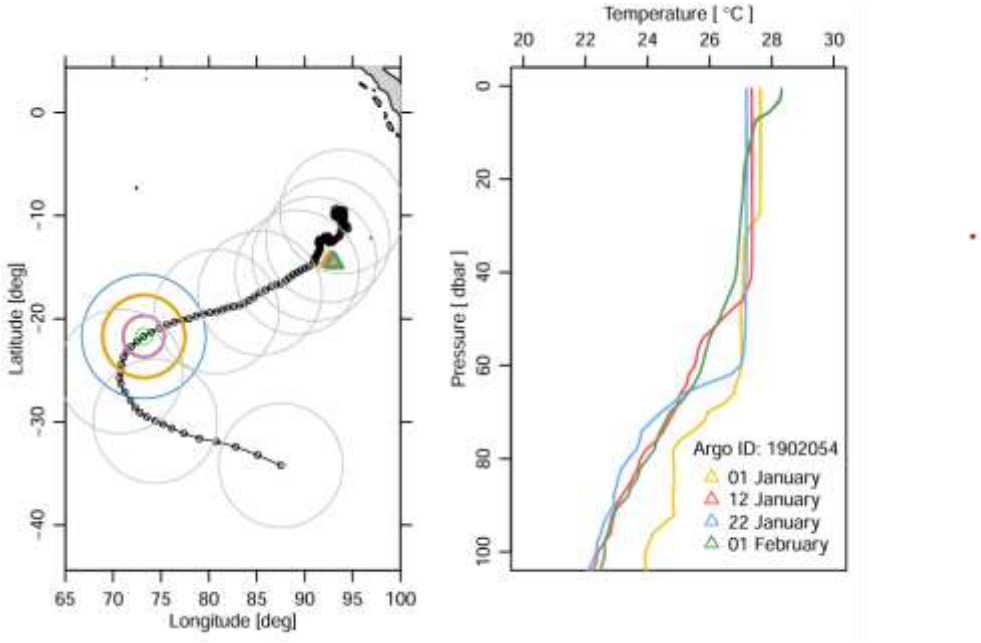

Figure 2. Temperature depth profiles [°C] of floats 1902054 in the Indian Ocean during TC Anggrek. The green cycle shows the day of maximum wind speed. The pink circle represents the 64 kt wind radius, the middle orange circle indicates the 50 kt wind radius and are shown for the day of maximum wind speed. The largest grey and blue circle correspond to the 34 kt wind radius and is shown daily.

Before TC **Lorna (Cat 2)**, MLT along most parts of its trajectory was anonymously warm, ranging from +1.5 °C to +3.0 °C (Figure 4; ARGO 5904722 (Ascending date: 30.04.2019)). By April 26, some water masses were anomalously cooler by –1.0 °C (Figure 5b), whereas other regions showed no significant anomalies (Figure 5a). In the satellite imagery, a cold anomaly is evident along the path of Lorna by April 26 reaching a maximum cooling of -2.3 °C and spanning an extent of up to 10° in latitude and longitude on April 26 (Figure 5b). The initial cooling is primarily located on the right side of the track and coincides with the slowest translation speed of TC Lorna by approximately 2 km/h on April 24 (Figures 4 and 5b, ARGO 5904722 (Ascending date: 30.04.2019, -2.0 °C)). Temperature anomalies were present prior to the passage of Lorna. Data from ARGO floats confirm these pre-existing cooling events and subsequent cooling, –0.4 °C (ARGO 2902586 (Ascending date:

 doi:10.20944/preprints202603.2120.v1

26.04.2019)) between the pre- and during-TC periods (Figure 4). Further cooling of –1.1 °C was recorded by ARGO 2902586 after Lorna passed, consistent with the satellite SST data (Figures 4 and 5c). By May 12, SST had returned to near-normal conditions (Figure 5c).

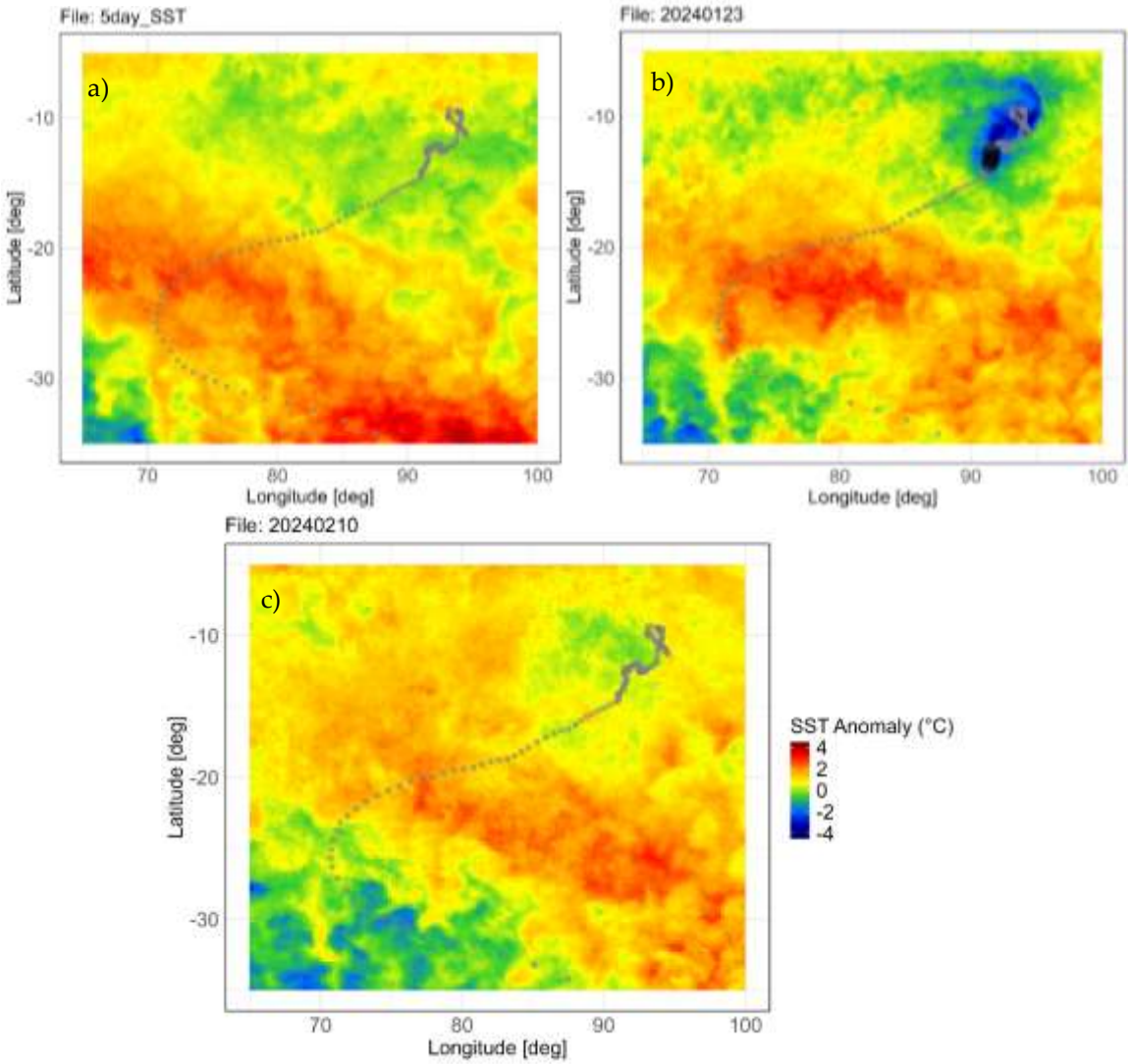

Figure 3. Sea Surface Temperature (SST) [°C] anomalies in the Indian Ocean during TC Anggrek, 2024. The track of TC Anggrek is shown in grey circles with the current positions (larger black circles). Satellite image a) shows a five-day composite prior to the passage of TC Anggrek. The track is shown for b) January and c) February 10, 2024.

For TC **Herman (Cat 4)**, SST cooling was less pronounced and shorter-lived than for the other five TCs. **Marian (Cat 3)** and **Riley (Cat 1)**, however showed similar SST cooling patterns, despite their different TC categories. **Amphan (Cat 5)** exhibited exceptionally warm pre-storm SSTs followed by strong cooling, with satellite SST data indicating drops by up to –4 °C. Overall, the strongest cooling occurred in cases when the translation speed was minimal and/or wind speeds were high (i.e., TC's intensity).

Both groups characterized by slow translation speeds ("slow translation speed & high wind" and "slow translation speed & low wind" in Figure 6) exhibit the most negative median SST anomalies (-0.4 °C and -0.5 °C, respectively), while only the group "fast & high wind" is characterized by a positive median of 0.3 °C (Figure 6).

 doi:10.20944/preprints202603.2120.v1

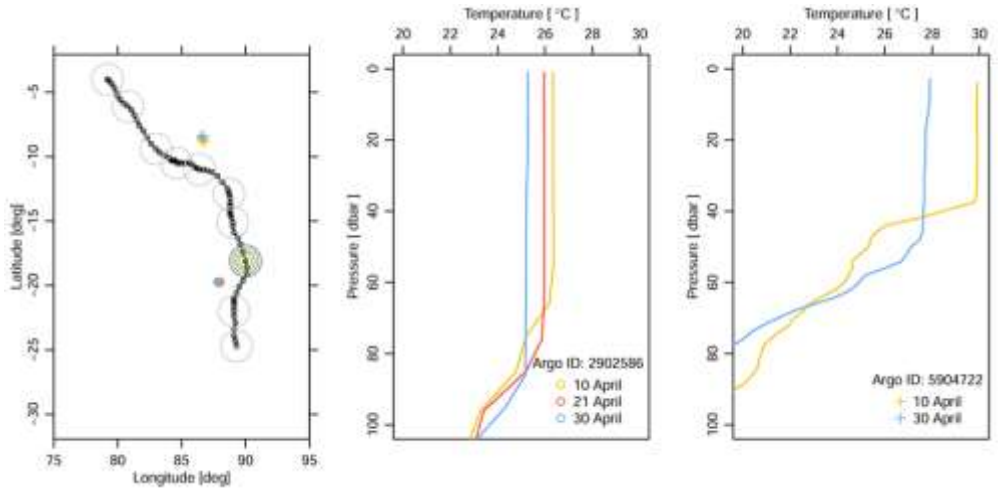

Figure 4. Temperature depth profiles of floats 2902586 and 5904722 in the Indian Ocean during TC Lorna 2019. The green circle shows the day of maximum wind speed. The pink circle represents the 64 kt wind radius, the middle orange circle indicates the 50 kt wind radius and are shown for the day of maximum wind speed. The largest grey and blue circle correspond to the 34 kt wind radius and is shown daily.

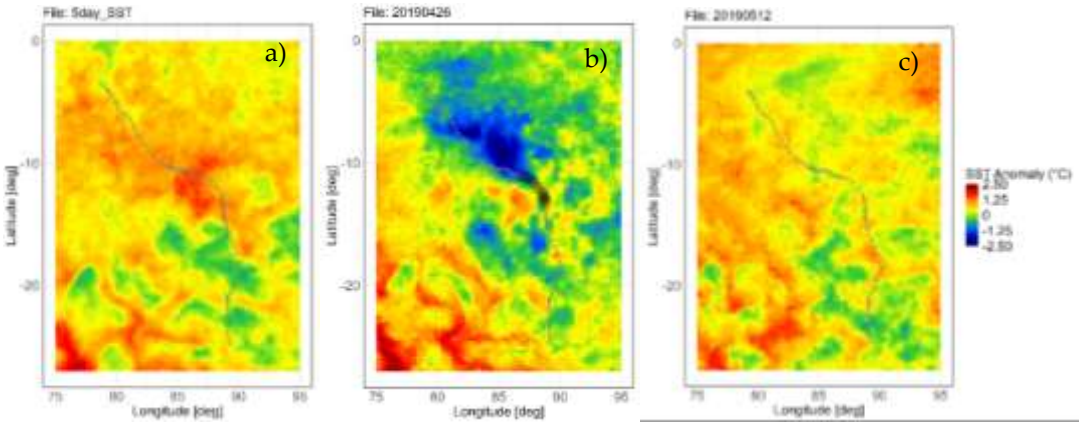

Figure 5. Sea Surface Temperature (SST) anomalies [°C] in the Indian Ocean during TC Lorna. The track of TC Lorna is shown in grey circles with current positions (larger black circles). Satellite image a) displays a five-day composite before the passage of TC Lorna. The track is shown for b) April 26 and c) May 12, 2019.

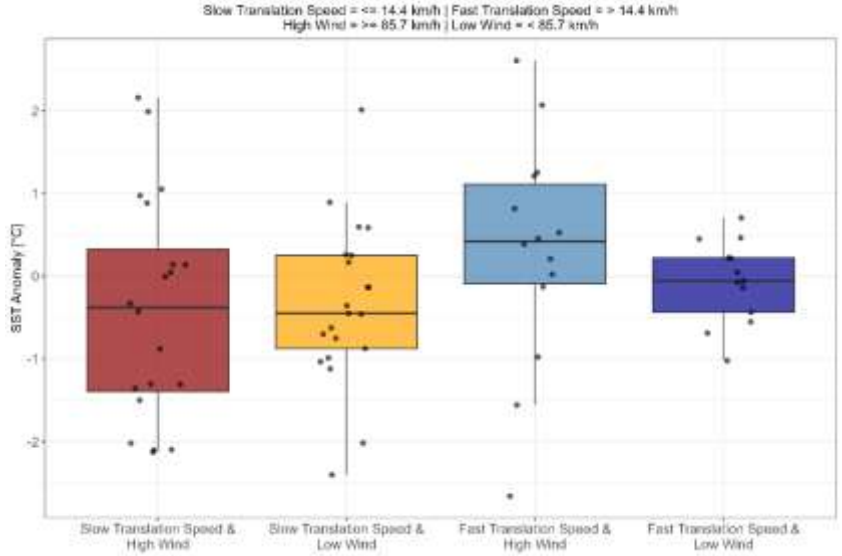

 doi:10.20944/preprints202603.2120.v1

Figure 6. Boxplot of SST anomalies [°C] grouped by translation speed ([km/h], slow vs. fast) and wind speed ([km/h], high vs. low). The "slow translation speed & high wind" group is illustrated by the red boxplot and includes SST anomalies measured with a translation speed of ≤ 14.4 km/h and wind speeds ≥ 85.7 km/h. The group "slow translation speed & low wind" is represented by the yellow boxplot and includes SST measured at a translation speed > 14.4 km/h and wind speeds < 85.7 km/h. The "fast translation speed & high wind" group is illustrated by the light blue boxplot and includes SST anomalies measured with a translation speed of > 14.4 km/h and wind speeds ≥ 85.7 km/h. The group "fast translation speed & low wind" is represented by the dark blue boxplot and includes SST measured at a translation speed > 14.4 km/h and wind speeds < 85.7 km/h. The figure illustrates the differences in the median (horizontal line within the boxes), variability, and the distribution of SST anomalies across the four groups.

The Shapiro-Wilk test indicates that all predefined groups follow a normal distribution (slow translation speed & high wind: $p = 0.194$; slow translation speed & low wind: $p = 0.820$; fast translation speed & high wind: $p = 0.832$; fast translation speed & low wind: $p = 0.938$). The one-way ANOVA reveals no significant differences in SST anomalies among the four groups ($F_{3,64} = 1.32$, $p = 0.28$). This is supported by pairwise comparisons using the Tukey HSD post hoc test, which showed no significant differences between groups (all adjusted p-values > 0.05). Overall, the groups with lower translation speeds and higher wind speeds exhibited the strongest negative SST anomalies, although these differences are not statistically significant.

3.2. Chlorophyll-a Response to Cyclones

Prior to the passage of TC **Anggrek**, enhanced absolute Chl-a concentrations were identified northeast of the TC's track (Figure 7a), but these signals had mostly dissipated before the onset of the TC. During the passage of TC Anggrek, a Chl-a anomaly developed along the storm track between January 12 and January 18. This anomaly became detectable for the first time on January 18, reaching a maximum of approximately 1.5 mg m^{-3} (Figure 7b). On January 26, another Chl-a anomaly was observed with a maximum of approximately 2.0 mg m^{-3} (Figure 7b). The initial anomaly (January 18) weakened by January 26, with reduced maximum concentrations of approximately 1.0 mg m^{-3} (Figure 7b). By February 15, Chl-a anomalies disappeared in the catchment area of TC Anggrek (Figure 7c).

No elevated Chl-a concentrations were detectable in the catchment area of TC Lorna 15 days before its passage (Figure 8a). Chl-a anomalies were first observed on April 26, with a maximum Chl-a anomaly of approximately 0.4 mg m^{-3} (Figure 8b). These anomalous conditions reached their maximum spatial extent on the right side of the track by April 26. No Chl-a anomalies were observed along the remaining track of TC Lorna (Figure 8b). By May 16, the Chl-a anomalies increased for a second time, probably due to favorable bloom conditions and not by upwelling processes of nutrient-rich water masses (Figure 8c). The magnitude of observed Chl-a anomalies after the passage of TC Lorna (Cat 1) was low compared to the other TCs, but persisted for a longer duration.

In comparison, the Chl-a anomalies observed during the passage of TC Herman were lower than those observed during TC Anggrek. A key finding is that the regions in which TCs Marian and Riley caused the greatest Chl-a anomalies were also those in which translation speeds were lowest and near-stationary behaviour occurred. TC Amphan as the strongest storm among those examined caused Chl-a anomalies nearly as high as those of TC Anggrek, with the strongest anomalies during the TCs lifetime coinciding with regions of reduced translation speed and pronounced SST cooling in both cases. For all six TCs, Chl-a anomalies were observed, coinciding with regions of SST cooling and reaching peak intensity and/or the lowest translation speed. The intensity and duration of visible Chl-a anomalies varied throughout the TCs.

The "slow translation speed & high wind" group shows the highest median Chl-a anomaly (0.1 ± 0.2 mg m^{-3}) with predominantly positive values (s. Figure 9). The "slow translation speed & low wind" group shows a lower positive median (0.02 ± 0.2 mg m^{-3}, Figure 9). In contrast, both "fast" groups are characterized by substantially lower median anomalies (0.002 ± 0.08 mg m^{-3} for high wind, 0.006 ± 0.05 mg m^{-3} for low wind; Figure 9).

 doi:10.20944/preprints202603.2120.v1

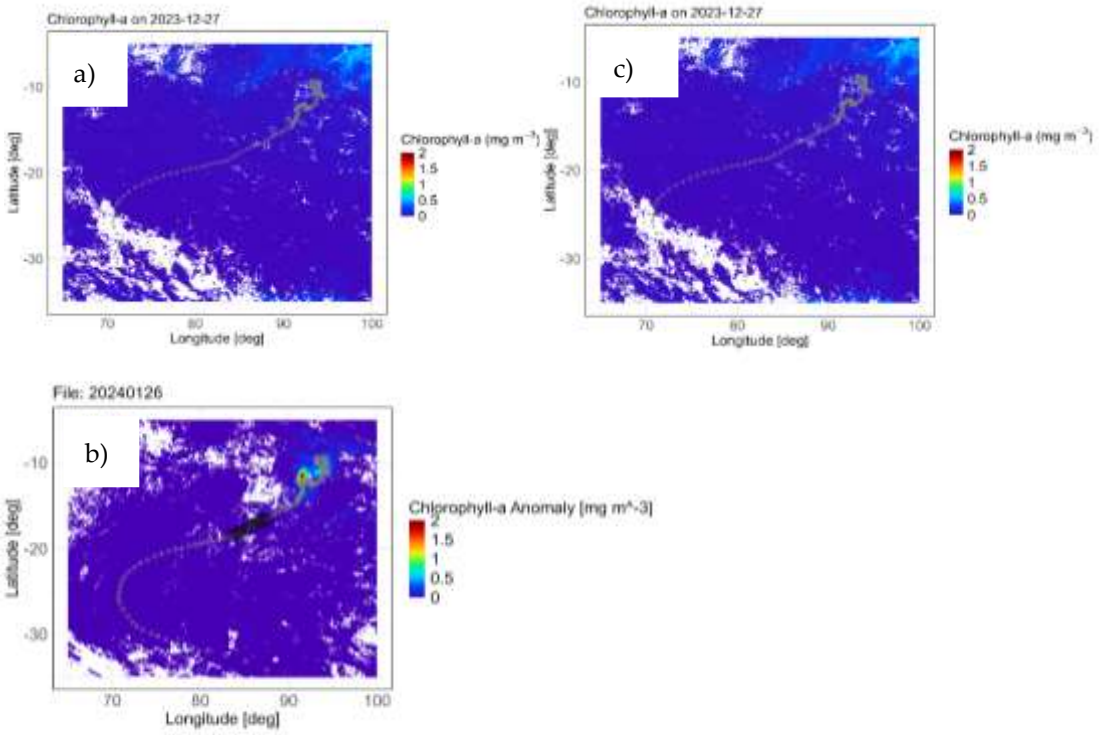

Figure 7. a) Chlorophyll-a concentration [mg m^{-3}] shown as a five-day composite in the Indian Ocean, representing conditions 16 days prior to the passage of TC Anggrek. The cyclone track corresponds to December 27, 2024. b) Chlorophyll-a anomalies [mg m^{-3}] during the passage of TC Anggrek on January 26, 2024. The track of TC Anggrek is indicated by grey circles, with the current cyclone position highlighted by larger black circles. c) Chlorophyll-a concentration [mg m^{-3}] on February 15, 2024, illustrating post-cyclone conditions.

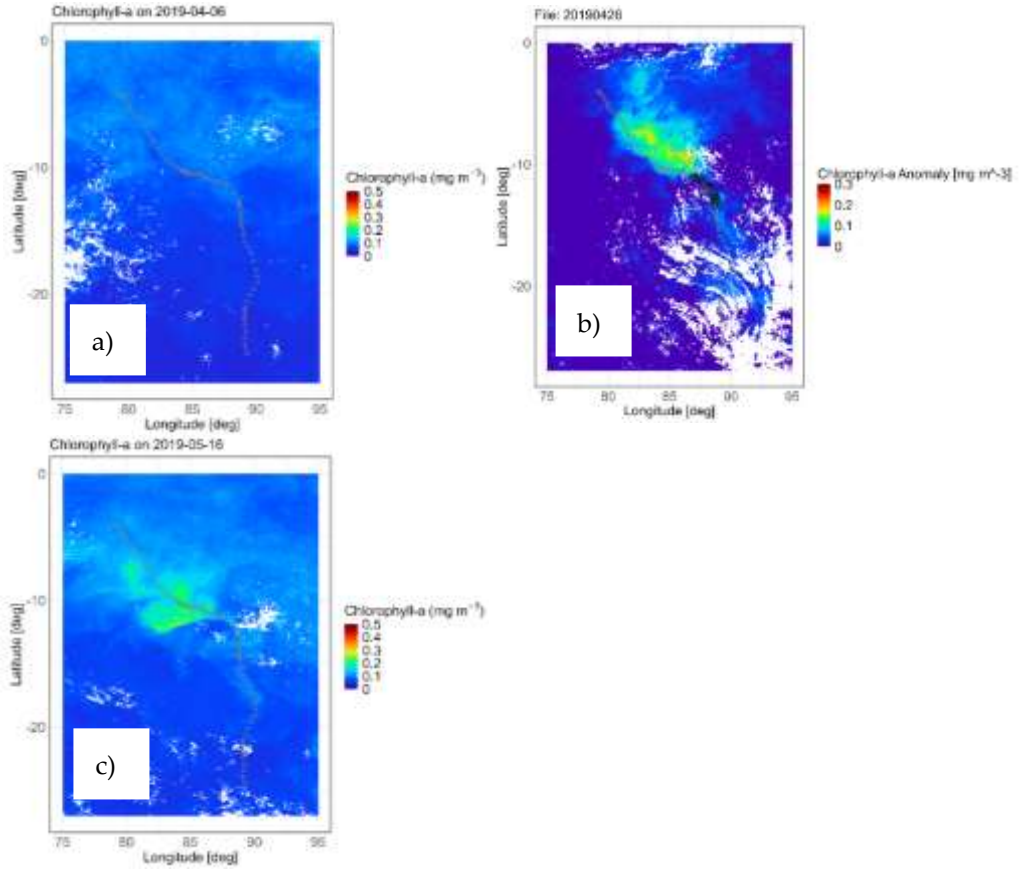

 doi:10.20944/preprints202603.2120.v1

Figure 8. a) Chlorophyll-a concentration [mg m^{-3}] shown as a five-day composite in the Indian Ocean, representing conditions 15 days prior to the passage of TC Lorna. The cyclone track corresponds to April 6, 2019. b) Chlorophyll-a anomalies [mg m^{-3}] during the passage of TC Lorna on April 26, 2019. The track of TC Lorna is indicated by grey circles, with the current cyclone position highlighted by larger black circles. c) Chlorophyll-a concentration [mg m^{-3}] on May 16, 2019, illustrating post-cyclone conditions.

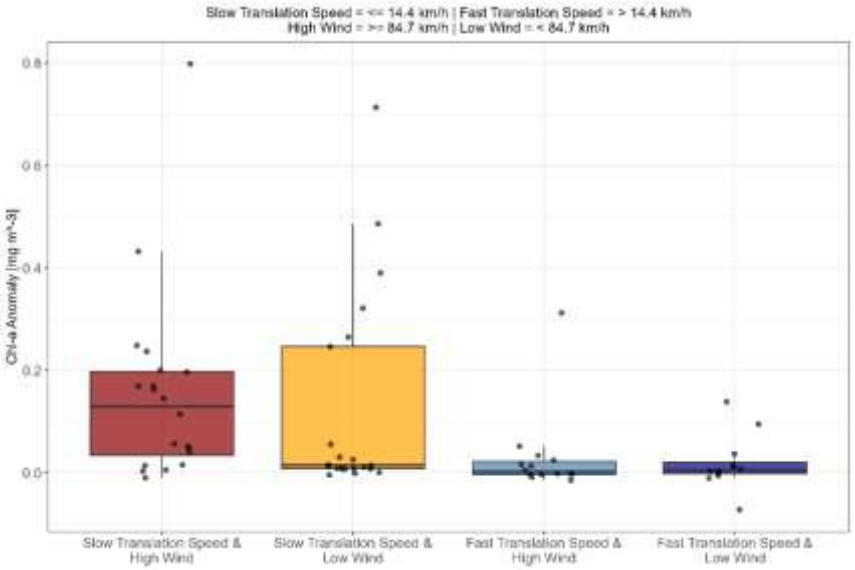

Figure 9. Boxplot of chlorophyll-a (Chl-a) anomaly [mg m^{-3}] grouped by translation speed ([km/h], slow vs. fast) and wind speed (km/h, high vs. low). The "slow translation speed & high wind" group is illustrated by the red boxplot and includes Chl-a anomalies measured with a translation speed of ≤ 14.4 km/h and wind speeds ≥ 85.7 km/h. The group "slow translation speed & low wind" is represented by the yellow boxplot and includes Chl-a anomalies measured at a translation speed > 14.4 km/h and wind speeds < 85.7 km/h. The "fast translation speed & high wind" group is illustrated by the light blue boxplot and includes Chl-a anomalies measured with a translation speed of >14.4 km/h and wind speeds ≥ 85.7 km/h. The group "fast translation speed & low wind" is represented by the dark blue boxplot and includes Chl-a anomalies measured at a translation speed > 14.4 km/h and wind speeds < 85.7 km/h. The figure illustrates the differences in the median (horizontal line within the boxes), variability, and the distribution of Chl-a anomalies across the four groups.

The Shapiro-Wilk test indicates that none of the groups follow a normal distribution (p-value > 0.05). Therefore, the Wilcoxon test was applied and indicates a statistically significant difference between the "slow translation speed & high wind" and "fast translation speed & high wind" groups ($p < 0.05$; $p = 0.001$). Similarly, a significant difference was observed between the groups "slow translation speed & low wind" and "fast translation speed & low wind" ($p = 0.03$). For the two groups, "slow translation speed & high wind" and "fast translation speed & high wind", similar observations were noted in the boxplot and therefore align with the results (Figure 9). In contrast, the results for "fast translation speed & low wind" and "fast translation speed & high wind" are less pronounced in the boxplot (Figure 9). Overall, the group with lower translation speeds and higher wind speeds includes the most positive Chl-a anomalies.

4. Discussion

The observed anomalous surface cooling can be attributed to the passages of TCs. The wind curl causes cold, nutrient-rich deep water to rise to the surface through the Ekman forcing [6,7,14]. This upwelling process was detected for all observed TCs, but with varying degrees, extents, and durations of cooling. A prerequisite for the formation of a TC is a SST higher than 26 °C [1,3–5]. Pre-

 doi:10.20944/preprints202603.2120.v1

TC SSTs ranged from 27.8 °C to 32 °C across all TCs. SST cooling typically occurs approximately one day after a TC passes, with recovery times varying among TCs, from a few days to several weeks [7].

The degree of cooling related to the characteristics of TCs depends on four factors, as outlined by Lin [10]: (i) the intensity of a TC, as wind forcing is the primary driver of ocean response, (ii) the translation speed and (iii) the size in vortex diameter, both of which determine the transit time, (iv) the pre-condition of the upper ocean and atmosphere, including warming state, stratification of the water column, and their energetic condition [10,14]. If any of these conditions divert from the most favorable state, a reduced SST cooling may be expected [1,7,10]. Hence, the cooling can range from 1 °C to 6 °C, and even up to 11 °C under the most favorable conditions [1,7]. Several studies stated that TCs with slower translation speeds have a longer exposure time, which induces more momentum on the ocean surface, resulting in a larger degree of upwelling and entrainment, leading to more negative anomalies [1,8,10,14].

Observed trends suggest that slower translation speeds combined with high wind intensity produce the most negative anomalies, followed by slower translation speeds and lower wind speeds. Similar relationships have been reported in previous studies [10,29]. The multiple correlation analysis conducted by Zhao & Wang [9] demonstrates the importance of both translation speed and intensity as key factors in determining the degree of upwelling and, consequently, the degree of SST cooling. Hence, it is concluded that the storm intensity influences the degree of negative SST anomalies. Previous studies also report increasing SST cooling with storm intensity, although this relationship is not strictly linear across TC categories [7,30].

This is supported by the ANOVA and subsequently the Tukey HSD comparisons, which indicate that translation speed and wind speed alone do not fully determine the extent of SST cooling, suggesting that TC intensity and translation speed are not the only factors that determine the extent of SST cooling. Against this background, it is notable that TC Herman (Cat. 4) induced a maximum SST cooling of only −3 °C, despite relatively low translation speeds, whereas Anggrek (Cat. 4) and Marian (Cat. 3) produced stronger cooling of −4 °C and −3.2 °C, respectively, under slower movement and elevated wind conditions. Variations in translation speed among these TCs were influenced by large-scale atmospheric steering, including subtropical ridges and mid-latitude troughs, which are known to modulate TC motion [31]. The background environment, including the wind field, affects translational speed. Reduced forward movement increases momentum transfer to the ocean surface, favoring stronger SST cooling, as seen in the TCs Anggrek and Marian. The shorter quasi-stationary phase of TC Herman, limited to a single day and associated with a translation speed of 6 km/h, indicates a shorter or less intense influence from steering pressure systems. As Lin [10] suggested, the cooling is also dependent on the stratification of the ocean. TCs Marian, Riley, and Herman were all influenced by the Indonesian Throughflow stratification, which is characterized by low salinity waters that enhance upper-ocean stratification and promote the formation of barrier layers [32–34]. A shallow and stable thermocline inhibits vertical mixing, thereby reducing the TC-induced cooling and increasing the possibility for further intensification of the TC [34,35]. Ummenhofer et al. [36] proposed salinity in the IO to vary throughout the monsoon season, resulting in different stratification and barrier layers. TCs Marian and Riley occurred during the boreal winter, which is between December and February, when stratification and barrier-layer thickness are reduced [37–39]. This may have led to pronounced SST cooling despite their moderate intensity [37,38]. In contrast, TC Herman developed during the boreal summer (June to September), corresponding to the Southwest Monsoon period in the northern IO, when stronger salinity stratification and a thicker barrier layer likely limited vertical mixing and reduced SST cooling, even under favorable wind and translation-speed conditions [1,10,34,37,39]. A similar mechanism applies to TC Amphan, which occurred during the pre-monsoon season, characterized by a thin or absent barrier layer, allowing stronger cooling of −3.6 °C, consistent with its high intensity [1]. Cooling observed prior to the passage of TCs Marian, Herman, and Lorna cannot be attributed to TC forcing, as they had not yet crossed the affected regions. This pre-existing cooling is likely linked to cold-core eddies, which are associated with low ocean heat content and can persist for several weeks. Such preconditioning by

 doi:10.20944/preprints202603.2120.v1

mesoscale ocean dynamics has been reported previously (ibid.). However, limited temporal and spatial resolution of ARGO float data restricts detailed interpretation in this study.

All TCs triggered an increase in Chl-a concentration at the surface. However, the strength and duration of the induced Chl-a increase differed between the individual TCs. The increase in Chl-a concentration is a typical response observed after the passage of a TC. This phenomenon is attributed to the upward propagation of deeper Chl-a maxima or new production [1]. This new production can result from vertical mixing and upwelling of cold, nutrient-rich water into the euphotic zone, or from increased terrestrial runoff and resuspension in coastal areas [14]. Zhao & Wang [9] analyzed multiple TCs in the South China Sea (1998-2015) and reported that increased Chl-a concentrations, hence a bloom occurs only if the TC forcing time exceeds the geostrophic adjustment time, the period needed for phytoplankton to respond to TC-induced physical changes, such as vertical mixing and nutrient supply. Consequently, the translation speed exerts a substantial influence on the enhancement of nutrients within the surface layer, thereby leading to elevated concentrations of Chl-a [9]. According to Lin [10], elevated Chl-a concentrations in the surface layer are most likely to occur when the TC does not encounter a pronounced warm-core eddy, reaches a category four or five with wind speeds between 125 kt and 145 kt, and has a sufficiently long transit time of at least 20 h. Such a transit time corresponds to a TC translation speed of ≤ 3.6 m/s (13.0 km/h) [10]. Furthermore, Zhao & Wang [9] concluded the ratio of the Chl-a concentration before and after the TC are influenced by SST, translation speed, and the intensity of a TC. Our results (Figure 9) with the Wilcoxon test indicate for the combined group of translation speed and wind intensity that slower translation speeds are associated with elevated positive anomalies. The significantly strongest positive anomalies were recorded for the group “slow speed & high wind”, followed by “slow speed & low wind”. As Russel & Horvat [6] showed, with a fast translation speed, the momentum on the ocean is too short, resulting in nutrients not being entrained into the euphotic zone; therefore, the promoted bloom cannot be induced. It confirms the findings of Zhao & Wang [9] that both translation speed and intensity are crucial factors for the degree of upwelling and entrainment. Thus, can serve as an indicator for the transport of cold, nutrient-rich water into the surface layer. A significant partial correlation between SST and Chl-a anomalies following the passage of TC, was demonstrated by Zhao &Wang [9], indicating the degree of upwelling can be determined by the degree of SST cooling. As discussed earlier, the results relating to SST, translation speed, and wind intensity indicate these factors influence the SST anomaly. Therefore, it can be concluded that the Chl-a anomalies are also dependent on them. Lin [10] concluded the precondition of the ocean determines the degree of the observed Chl-a bloom. The results from the satellite imagery further support the significant partial correlation observed by Zhao & Wang [9].

For each TC, the region where SST cooling was observed coincided with the regions of enhanced Chl-a anomalies. TC Amphan exhibited the strongest response with a Chl-a anomaly of 3.0 mg m^{-3}, and coinciding with its lowest translation speed, highest wind intensity, and pronounced SST cooling. This response is consistent with previous studies from the Bay of Bengal and supports the role of TC-induced vertical mixing and upwelling in enhancing surface phytoplankton biomass [1]. In contrast, TC Lorna induced a comparatively weak Chl-a anomaly of 0.3 mg m^{-3}, but the elevated concentrations persisted substantially longer than for the other TCs, which generally returned to background conditions within two to three weeks [14]. The persistent Chl-a anomaly can be attributed to the existence of a slow-growing community which is limited in its growth by the nutrient iron [3]. Another possible explanation for the persistent Chl-a bloom could be the influence of a vortex generated by the TC Lorna. As Lu et al. [40] have shown, TCs can exert a significant influence on oceanic eddies, thereby altering their structural properties. This, in turn, can affect upwelling currents and the dynamic process of eddy adjustment [40,41]. The observed Chl-a anomalies ranged from 0.2 mg m^{-3} to 3.0 mg m^{-3} and is within the reported values from other studies [10,11,24,42]. However, several studies indicate a strong dependency of the increase in Chl-a concentrations on TC characteristics and ocean preconditions, and should therefore not be generalized [3,10]. For TCs Marian and Riley, a pre-bloom was observed before the passage of the TCs, and the pre-existing

 doi:10.20944/preprints202603.2120.v1

bloom was intensified by the TC's passages. For these regions, it can therefore be assumed that these are pre-existing phytoplankton communities being promoted by upwelling and entrainment [7,9,14]. The oceanic response to TCs is subject to observational constraints. Maximum SST cooling may occur one to two days after TC passage and may therefore be underestimated when extracted along daily storm tracks. Subsurface thermal responses and associated nutrient fluxes cannot be fully resolved due to the limited temporal and spatial coverage of ARGO floats. In addition, satellite-derived surface Chl-a is affected by cloud cover and temporal averaging, which smooth out dynamics in bloom developments and, therefore, fast oceanic responses after TC passages. The study is limited by sample size, the restricted availability of ARGO floats, and the temporal resolution of satellite-derived Chl-a data, which constrain the ability to capture delayed oceanic responses to TCs fully. Future work should combine larger TC samples with improved in situ and satellite observations across multiple ocean basins.

5. Conclusions

This study demonstrates that TC-induced SST cooling and surface Chl-a enhancement are strongly modulated by translation speed and wind intensity and are also influenced by oceanic preconditions such as stratification. The analysis of six TCs showed that those with a low translation speed (≤ 4 m/s) produce the most significant negative SST anomalies. Enhanced Chl-a anomalies spatially coincided with SST cooling, supporting the use of SST cooling as a proxy for TC-induced upwelling and Chl-a blooms. Overall, slower translation speeds and higher wind speeds produced the most significant anomalies, although other factors also contributed.

These findings are particularly significant in the context of future climate projections. The IPCC reports a trend toward more frequent and intense TC with higher wind speeds, slower translation speeds, and heavier rainfall. Slower-moving TCs prolong surface forcing, leading to enhanced ocean cooling and changes in heat transport within the cold wake, which in turn can affect cloud cover. The combination of increased precipitation and slower translation speeds is likely to alter upper-ocean stratification and promote higher Chl-a concentrations in the IO. Such changes may trigger cascading effects in marine ecosystems, including shifts in plankton community composition, altered trophic interactions, expansion of oxygen-depleted zones, and an increased likelihood of harmful algal blooms, ultimately destabilizing oligotrophic food webs.

These results provide valuable insights into the relationships among SST and Chl-a anomalies, translation speed, and wind intensity, which are increasingly relevant as TC occurrence is expected to increase due to climate change. Understanding where a TC might slow down and remain relatively stationary could support early warning systems and inform climate adaptation and disaster risk management strategies.

Supplementary Materials: The following supporting information can be downloaded at the website of this paper posted on Preprints.org.

Author Contributions: Conceptualization, P.S.K. and O.W.; methodology, P.S.K., S.M.A., O.W.; validation, S.M.A.; formal analysis, P.S.K.; investigation, P.S.K.; resources, O.W.; data curation, P.S.K.; writing—original draft preparation, P.S.K.; writing—review and editing, S.M.A., O.W.; visualization, P.S.K. and S.M.A.; supervision, O.W.; project administration, O.W.; funding acquisition, O.W. All authors have read and agreed to the published version of the manuscript.

Funding: The publication of this work was made possible with the internal funding provided the University of Oldenburg.

Data Availability Statement: All data used are secondary data from multiple sources. These data are all publicly available data. All sources have been stated in the methods section with the adequate links and DOIs also provided.

 doi:10.20944/preprints202603.2120.v1

Acknowledgments: I am very thankful to the NASA's Jet Propulsion Laboratory and the Physical Oceanography Distributed Active Archive (PO. DAAC) for the provision and dissemination of the satellite data used in this study. The data were provided in line with NASA's Earth Science Program Data and Information Policy, enabling open access to scientific research. I also would like to express my gratitude to the OceanColor Group, the European Space Agency, the NASA Global Modeling and Assimilation Office, NASA Goddard Earth Sciences Data Information Services Center, the Euro-Argo European Research Infrastructure Consortium, and the ARGO Community for assimilation and sharing data. Grammarly (v1.2.225.1809) was used to proofread and correct the manuscript's language.

Conflicts of Interest: The authors declare no conflicts of interest. The funders had no role in the design of the study; in the collection, analyses, or interpretation of data; in the writing of the manuscript; or in the decision to publish the results.

Abbreviations

The following abbreviations were used in the manuscript:

TC	Tropical Cyclone
SST	Sea Surface Temperature
Chl-a	Chlorophyll-a
IO	Indian Ocean
ARGO	Array for Real-Time Geostrophic Oceanography
IBTrACS	International Best Track Archive for Climate Stewardship
GHRSST	Group for High Resolution Sea Surface Temperature
MUR	Multi-scale Ultra-high Resolution
JPL	Jet Propulsion Laboratory
PO.DAAC	Physical Oceanography Distributed Active Archive Center
OC-CCI	Ocean Colour Climate Change Initiative
ESA	European Space Agency
MERRA-2	Modern-Era Retrospective analysis for Research and Applications, Version 2
GMAO	Global Modeling and Assimilation Office
GES DISC	Goddard Earth Sciences Data and Information Services Center
ANOVA	Analysis of Variance
HSD	Honestly Significant Difference

References

1. Singh, V.K.; Roxy, M.K. A review of ocean-atmosphere interactions during tropical cyclones in the north Indian Ocean. *Earth-Science Reviews* **2022**, *226*, 1–23, doi:10.1016/j.earscirev.2022.103967.
2. Yamaguchi, M.; Chan, J.C.L.; Moon, I.-J.; Yoshida, K.; Mizuta, R. Global warming changes tropical cyclone translation speed. *Nat Commun* **2020**, *11*, 47, doi:10.1038/s41467-019-13902-y.
3. Neun, S.; Jacob, J.; Wurl, O. Upper Ocean Responses to the Tropical Cyclones Ida and Felicia (2021) in the Gulf of Mexico and the Eastern North Pacific. *Remote Sensing* **2022**, *14*, doi:10.3390/rs14215520.
4. Henderson-Sellers, A.; Zhang, H.; Berz, G.; Emanuel, K.; Gray, W.; Landsea, C.; Holland, G.; Lighthill, J.; Shieh, S.-L.; Webster, P.; et al. Tropical Cyclones and Global Climate Change: A Post-IPCC Assessment. *Bull. Amer. Meteor. Soc.* **1998**, *79*, 19–38, doi:10.1175/1520-0477(1998)079<0019:TCAGCC>2.0.CO;2.
5. Mavume, A.F.; Rydberg, L.; Rouault, M.; Lutjeharms, J.R. Climatology and Landfall of Tropical Cyclones in the South- West Indian Ocean. *West Ind. Oc. J Mar. Sci.* **2010**, *8*, doi:10.4314/wiojms.v8i1.56672.
6. Russell, P.; Horvat, C. Extreme South Pacific Phytoplankton Blooms Induced by Tropical Cyclones. *Geophysical Research Letters* **2023**, *50*, doi:10.1029/2022GL100821.
7. Zhang, H.; He, H.; Zhang, W.-Z.; Di Tian. Upper ocean response to tropical cyclones: a review. *Geoscience Letters* **2021**, *8*, 1, doi:10.1186/s40562-020-00170-8.
8. Price, J.F. Upper Ocean Response to a Hurricane. *J. Phys. Oceanogr.* **1981**, *11*, 153–175, doi:10.1175/1520-0485(1981)011<0153:UORTAH>2.0.CO;2.

 doi:10.20944/preprints202603.2120.v1

9. Zhao, H.; Wang, Y. Phytoplankton Increases Induced by Tropical Cyclones in the South China Sea During 1998–2015. *J. Geophys. Res.* **2018**, *123*, 2903–2920, doi:10.1002/2017JC013549.
10. Lin, I.-I. Typhoon-induced phytoplankton blooms and primary productivity increase in the western North Pacific subtropical ocean. *J. Geophys. Res.* **2012**, *117*, doi:10.1029/2011JC007626.
11. Menkes, C.E.; Lengaigne, M.; Lévy, M.; Ethé, C.; Bopp, L.; Aumont, O.; Vincent, E.; Vialard, J.; Jullien, S. Global impact of tropical cyclones on primary production. *Global Biogeochemical Cycles* **2016**, *30*, 767–786, doi:10.1002/2015GB005214.
12. IPCC. *Climate Change 2021 – The Physical Science Basis: Working Group I Contribution to the Sixth Assessment Report of the Intergovernmental Panel on Climate Change*; Cambridge University Press: Cambridge, 2023.
13. Weather and Climate Extreme Events in a Changing Climate. In *Climate Change 2021 – The Physical Science Basis: Working Group I Contribution to the Sixth Assessment Report of the Intergovernmental Panel on Climate Change*; IPCC, Ed.; Cambridge University Press: Cambridge, 2023; pp 1513–1766, ISBN 9781009157889.
14. Wurl, O.; Meyerjürgens, J. Intense Cooling of the Upper Ocean with the Merging of Tropical Cyclones: A Case Study in the Southeastern Indian Ocean. *su-j-tadmo* **2024**, *76*, doi:10.16993/tellusa.4083.
15. Kossin, J.P. A global slowdown of tropical-cyclone translation speed. *Nature* **2018**, *558*, 104–107, doi:10.1038/s41586-018-0158-3.
16. Jha, R.K.; Bhaskar, T.U. Generation and Assessment of ARGO Sea Surface Temperature Climatology for the Indian Ocean Region. *Oceanologia* **2023**, *65*, 343–357, doi:10.1016/j.oceano.2022.08.001.
17. Yu, J.; Lv, H.; Tan, S.; Wang, Y. Tropical Cyclone-Induced Sea Surface Temperature Responses in the Northern Indian Ocean. *JMSE* **2023**, *11*, 2196, doi:10.3390/jmse11112196.
18. Knapp, K.R.; Kruk, M.C.; Levinson, D.H.; Diamond, H.J.; Neumann, C.J. The International Best Track Archive for Climate Stewardship (IBTrACS). *Bull. Amer. Meteor. Soc.* **2010**, *91*, 363–376, doi:10.1175/2009BAMS2755.1.
19. Gahtan, J.; Knapp, K.R.; Schreck, C.J., III; Diamond, H.J.; Kossin, J.P.; Kruk, M.C. *International Best Track Archive for Climate Stewardship (IBTrACS) Project, Version 4.01*, 2024.
20. Roemmich, D.; Johnson, G.C.; Riser, S.; Davis, R.; Gilson, J.; Owens, W.B.; Garzoli, S.L.; Schmid, C.; Ignaszewski, M. The Argo Program: Observing the Global Ocean with Profiling Floats. *Oceanography* **2009**, *22*, 34–43.
21. NASA/JPL. *GHRSST Level 4 MUR 0.25deg Global Foundation Sea Surface Temperature Analysis (v4.2);* NASA Physical Oceanography Distributed Active Archive Center, 2019.
22. Yang, C.; Leonelli, F.E.; Marullo, S.; Artale, V.; Beggs, H.; Nardelli, B.B.; Chin, T.M.; Toma, V. de; Good, S.; Huang, B.; et al. Sea Surface Temperature Intercomparison in the Framework of the Copernicus Climate Change Service (C3S). *Journal of Climate* **2021**, *34*, 5257–5283, doi:10.1175/JCLI-D-20-0793.1.
23. Chin, T.M.; Vazquez-Cuervo, J.; Armstrong, E.M. A multi-scale high-resolution analysis of global sea surface temperature. *Remote Sensing of Environment* **2017**, *200*, 154–169, doi:10.1016/j.rse.2017.07.029.
24. Zheng, G.M.; Tang, D.L. Offshore and nearshore chlorophyll increases induced by typhoon winds and subsequent terrestrial rainwater runoff. *Mar. Ecol. Prog. Ser.* **2007**, *333*, 61–74, doi:10.3354/meps333061.
25. Zhao, H.; Shao, J.; Han, G.; Yang, D.; Lv, J. Influence of Typhoon Matsa on Phytoplankton Chlorophyll-a off East China. *PLoS One* **2015**, *10*, e0137863, doi:10.1371/journal.pone.0137863.
26. Sathyendranath, S.; Jackson, T.; Brockmann, C.; Brotas, V.; Calton, B.; Chuprin, A.; Clements, O.; Cipollini, P.; Danne, O.; Dingle, J.; et al. *ESA Ocean Colour Climate Change Initiative (Ocean_Colour_cci): Version 6.0, 4km resolution data*, 2023. Available online: https://dx.doi.org/10.5285/5011d22aae5a4671b0cbc7d05c56c4f0.
27. Global Modeling and Assimilation Office; Pawson, S. *MERRA-2 inst6_3d_ana_Np: 3d,6-Hourly,Instantaneous,Pressure-Level,Analysis,Analyzed Meteorological Fields V5.12.4*, 2015 (accessed on 13 July 2025).
28. Bosilovich, M.G.; Lucchesi, R.; Suarez, M. *MERRA-2: File Specification.* Available online: https://disc.gsfc.nasa.gov/datasets/M2I6NPANA_5.12.4/summary (accessed on 13 July 2025).
29. Dare, R.A.; McBride, J.L. Sea Surface Temperature Response to Tropical Cyclones. *Monthly Weather Review* **2011**, *139*, 3798–3808, doi:10.1175/MWR-D-10-05019.1.
30. Lloyd, I.D.; Vecchi, G.A. Observational Evidence for Oceanic Controls on Hurricane Intensity. *Journal of Climate* **2011**, *24*, 1138–1153, doi:10.1175/2010JCLI3763.1.

 doi:10.20944/preprints202603.2120.v1

31. Peng, S.; Qian, Y.-K.; Lai, Z.; Hao, S.; Chen, S.; Xu, H.; Wang, D.; Xu, X.; Chan, J.C.L.; Zhou, H.; et al. On the mechanisms of the recurvature of super typhoon Megi. *Scientific Reports* **2014**, *4*, 4451, doi:10.1038/srep04451.
32. Schott, F.A.; Xie, S.-P.; McCreary, J.P. Indian Ocean circulation and climate variability. *Reviews of Geophysics* **2009**, *47*, doi:10.1029/2007RG000245.
33. Gordon, A.L.; Sprintall, J.; van Aken, H.M.; Susanto, D.; Wijffels, S.; Molcard, R.; Ffield, A.; Pranowo, W.; Wirasantosa, S. The Indonesian throughflow during 2004–2006 as observed by the INSTANT program. *Dynamics of Atmospheres and Oceans* **2010**, *50*, 115–128, doi:10.1016/j.dynatmoce.2009.12.002.
34. Peng, S.; Wang, Q. Fast Enhancement of the Stratification in the Indian Ocean over the Past 20 Years. *Journal of Climate* **2024**, *37*, 2231–2245, doi:10.1175/JCLI-D-23-0255.1.
35. Feng, M.; Zhang, N.; Liu, Q.; Wijffels, S. The Indonesian throughflow, its variability and centennial change. *Geoscience Letters* **2018**, *5*, 3, doi:10.1186/s40562-018-0102-2.
36. Ummenhofer, C.C.; Murty, S.A.; Sprintall, J.; Lee, T.; Abram, N.J. Heat and freshwater changes in the Indian Ocean region. *Nat Rev Earth Environ* **2021**, *2*, 525–541, doi:10.1038/s43017-021-00192-6.
37. Gordon, A.L.; Susanto, R.D.; Vranes, K. Cool Indonesian throughflow as a consequence of restricted surface layer flow. *Nature* **2003**, *425*, 824–828, doi:10.1038/nature02038.
38. Xu, J. Change of Indonesian Throughflow outflow in response to East Asian monsoon and ENSO activities since the Last Glacial. *Science China Earth Sciences* **2014**, *57*, 791–801, doi:10.1007/s11430-014-4845-0.
39. Wang, B. *The Asian Monsoon;* Praxis Publishing Ltd. Chichester UK: Berlin, Heidelberg, 2006, ISBN 9783540377221.
40. Lu, Z.; Wang, G.; Shang, X. Response of a Preexisting Cyclonic Ocean Eddy to a Typhoon. *J. Phys. Oceanogr.* **2016**, *46*, 2403–2410, doi:10.1175/JPO-D-16-0040.1.
41. Liu, F.; Tang, S. Influence of the Interaction Between Typhoons and Oceanic Mesoscale Eddies on Phytoplankton Blooms. *J. Geophys. Res.* **2018**, *123*, 2785–2794, doi:10.1029/2017JC013225.
42. Lin, I.; Liu, W.T.; Wu, C.-C.; Wong, G.T.F.; Hu, C.; Chen, Z.; Liang, W.-D.; Yang, Y.; Liu, K.-K. New evidence for enhanced ocean primary production triggered by tropical cyclone. *Geophysical Research Letters* **2003**, *30*, doi:10.1029/2003GL017141.